INTERNATIONAL ASSOCIATION OF HYDROGEOLOGISTS

MEMOIRES

VOLUME XVII PART 2 PROCEEDINGS

HYDROGEOLOGY OF ROCKS OF LOW PERMEABILITY

TUCSON, ARIZONA, CONGRESS

UNITED STATES OF AMERICA

Published by a Committee of U.S.A. Members of the

International Association of Hydrogeologists

1985

A NEW CONTINUUM APPROACH FOR MODELING DISPERSION IN FRACTURED MEDIA

F.W. Schwartz
Dept. of Geology, Univ. of Alberta, Edmonton, Canada
L. Smith
Dept. of Geological Sciences, Univ. of British Columbia, Vancouver, Canada

Abstract

Continuum models in general provide the only practical approach to modeling dispersion in large, fractured rock systems. However, the conventional approaches based on a simple diffusional model of dispersion suffer from important limitations in representing the dispersion process. A new continuum approach has been developed that more realistically accounts for the influence of fractures and fracture geometries on the pattern of dispersion. The technique involves particle tracking where the particular motion of a large number of reference particles in the continuum is determined by the statistical characteristics of the network and specific features of low velocities in fractures. Detailed information on the pattern of directed random motion of particles requires the use of a discrete-fracture, submodel with a fracture geometry similar to that envisioned for the continuum model. In practice, the domain for the discrete model would be much smaller in size and contain many fewer intersections than the continuum model. By comparing breakthrough curves for discrete models and continuum models of the same system we have been able to demonstrate the validity and usefulness of this modeling procedure. The application of this approach included here is used to illustrate the potential applicability of the approach to a much larger two-dimensional system.

INTRODUCTION

This paper describes progress in the development of a new continuum approach for modeling transport in fractured rock systems. The method includes many of the best features of well-known discrete and continuum models (summarized in Schwartz et al., 1983) to produce a modeling methodology for large-scale systems. In the new approach, the influence of fractures on mass transport is accounted for much more realistically than in other continuum models. Following is a discussion of the modeling approach, which includes its numerical implementation and verification, and an application to a hypothetical transport problem.

Although our approach is applicable to both two and three-dimensional systems, the discussion here is restricted to two-dimensional systems. A companion paper (Smith et al., this volume) describes the three-dimensional, discrete-fracture model, which is one of the key elements necessary for the extension of this approach to three-dimensional systems.

METHODOLOGY

The essence of the method is to formulate the spread of the contaminant as a random-walk problem. Mass transport is simulated by the directed motion of a large number of reference particles. In this respect, it is generally the same as other continuum models used to simulate transport in porous media (Ahlstrom et al., 1977; Schwartz, 1977; Schwartz and Donath, 1980) and fractured media (Schwartz et al., 1983;

Smith and Schwartz, 1984). Where it does differ from these other approaches is in the way the reference particles are moved in order to mimic the unique patterns of mass transport developed as a consequence of the fracture geometry. In the moving particle models refered to above, the particle motion includes deterministic and random components, which are always related to the velocity of groundwater flow and the character of dispersion. In the new continuum method, particle motion is much more complex due to the variable geometry of the fracture network. As a consequence, the character of the random motion must be determined as part of the simulation problem. Actual particle motion is characterized from simulations of mass transport in discrete networks of fractures. Thus, our approach requires the use of discrete models as a preliminary to the continuum modeling.

In practice, one or more sub-domains of a very much larger continuum (Fig. 1) is selected for the discrete fracture modeling. This sub-domain is assumed to be oriented parallel to the direction of mean groundwater flow. Fractures in a two-dimensional sub-domain are represented as linear features. The two sides of the sub-domain are assumed to act as no-flow boundaries, and the ends are assumed to be constant head boundaries. Given these boundary conditions and a permeable network of fractures, groundwater will flow in the system.

The basic approach for modeling mass transport in a discrete network of this kind has been discussed in earlier work (Schwartz et al., 1983). Briefly, this approach involves generating a single realization of a fracture network by sampling probability distributions describing the occurence of fractures within a rock. Fractures are specified in terms of their location in space, their orientation, length and aperture. Depicted in Figure 2 is an example of the kind of fracture network that is generated within a sub-domain 62.25 m long and 21 m wide. The network consists of two orthogonal sets of fractures in this case aligned parallel (set 1) and perpendicular to the mean hydraulic gradient (set 2). The network is formed by adding 180 fractures in each of two sets to the sub-domain. Fracture lengths are sampled from a truncated negative exponential distribution and fracture apertures from a lognormal distribution.

In order for statistics on particle motion within the domain to be valid within the larger continuum, mass transport in the sub-domain must be ergodic. In other words, mass transport through the discrete network must be independent of the geometry of any particular realization but dependent on the overall statistical features of the network. The networks that we considered in earlier studies (Schwartz et al., 1983; Smith and Schwartz, 1984) all tended to be non-ergodic. Often there were considerable differences in the breakthrough curves from realization to realization. The non-ergodic behavior results from the relatively low fracture densities. Thus, it has been necessary in this study to alter the computer code to handle a much larger number of fracture intersections. In a typical simulation of the kind shown in Figure 2, there are approximately 1344 fracture intersections.

Another less obvious constraint that the requirement of ergodicity imposes on our approach relates to the minimum size of the sub-domain. In rock masses with relatively sparse fractures, the size of the sub-domain will be larger than rocks with relatively dense fractures. Work is currently underway to look at the question of how to determine the size of the sub-domain. However, it is important to realize that the modeler cannot arbitrarily choose the size of the sub-domain.

Because of limitations in the discrete fracture model, we have not been able to generate truly ergodic networks. At least for fracture sets that are parallel and perpendicular to the mean hydraulic gradient, there are minor changes in the transport behavior from realization to realization. As will become clear shortly, this slight non-ergodic behavior does influence the accuracy of the modeling approach applied to the continuum.

In the process of verifying the modeling concept, we have developed two different approaches to statistically characterize the particle motion. The first of these approach assumes that the discrete submodel is ergodic, while the second does not depend upon this assumption.

Approach 1 - Total Particle Statistics

In the first approach, the entire population of moving reference particles (usually 500) is used to compile probability distributions on the negative logarithm of the seepage velocities in the three main transport directions (1 up, 3 down, and 2 downstream) and the direction of particle movement at the fracture intersections. The velocity distributions are based on a substantial number of observations because each particle experiences from 50-100 velocity changes in moving through the fracture network. Each distribution is normalized by dividing by the logmean velocities ($-v_1$, $-v_2$, $-v_3$).

In addition to providing these distributions, the sub-domain is also used to provide the distributions on fracture lengths for both sets. These two distributions are formed from fractures that are actually sampled by the swarm of reference particles moving through the network. Because the reference particles are spread along the entire upstream boundary and sample many of the different fractures in the network, the distributions formed in this way do not differ very much from distributions formed from all of the fractures in each set. We have however chosen to be consistent by collecting all necessary statistics from the moving particles themselves.

The only other information required before moving to the continuum is an estimate of the equivalent logmean advective velocity ($-v_e$) across the domain. This velocity is estimated from the population of reference particles where the length of the sub-domain is divided by the transit time for individual particles to yield an equivalent velocity for each particle. Establishing a relationship between $-v_e$ and $-v_1$, $-v_2$, $-v_3$ will be necessary because in the continuum only equivalent parameters are available.

Let us now consider in detail how the statistics collected from the sub-domain can be used to describe particle motion within the continuum. The first step is to generate probability distributions on seepage velocities in the three transport directions appropriate for flow conditions in the continuum. Given estimates of the effective hydraulic conductivity (K_e) and effective porosity (θ_e) for the fractured rock, and the hydraulic gradient, it is possible to calculate an equivalent logmean velocity ($-v_e$) for the continuum. The hydraulic gradient is assumed to be known for the simple cases considered here. In more complex situations, the hydraulic gradient will be calculated from a continuum flow model. Values of $-v_1$, $-v_2$ and $-v_3$ for the continuum are estimated from relationships established in the discrete sub-domain as follows:

$$-v_1 = -v_e \cdot v_1/v_e \; : \; -v_2 = -v_e \cdot v_2/v_e \; : \; -v_3 = -v_e \cdot v_3/v_e \quad (1)$$

These means together with the normalized distributions of velocity from the discrete system provide the basis for estimating the probability distribution of the seepage velocities in the three transport directions in the continuum.

We are finally able with this information to move particles one at a time from the inflow boundary of the system to the outflow boundary. Following are the steps involved:

i) define a moving reference particle at the inflow boundary,

ii) sample the distribution to determine the direction of particle motion 1, 2, or 3 (for the first step the choice is constrained to the downstream direction 2)

iii) sample the appropriate length distribution to determine the distance to the next decision point or end of the continuum whichever is less,

iv) sample the velocity distribution appropriate for the given direction and calculate the time required to reach the decision point,

v) calculate the cumulative travel time

vi) return to (ii).

Note that the travel in directions 1 and 3 is limited by the top and bottom boundaries of the continuum. Steps ii) to vi) are repeated until the reference particle reaches the outflow end of the system. The elapsed time is saved to prepare a breakthrough curve for all of the particles. Because only physical transport occurs in the system, the particles can be moved independently from one another. However in

practice, there is not much more difficulty in moving the entire swarm of particles in given time steps.

What should be apparent is that as reference particles move through the continuum their motion mimics the way they move in the discrete network. Each particle in the continuum however will follow a different path because the fracture network does not exist in a discrete form. One important feature of the continuum approach is that it is not limited in the number of decision points or fracture intersections that can be included.

A simple procedure has been developed to verify that mass transport in the continuum accurately replicates the unique features observed for the discrete system. For this test, we have made the sizes of the domain for the continuum and discrete sub-model identical (62.25 x 21.0 m). Thus it is possible to compare breakthrough curves that result in both cases directly. These results are shown in Figure 3. They show that both approaches yield similar results. Of particular note is the shape of the curves at later times where the continuum model has successfully reproduced the long tails that can develop in networks of this type (Schwartz et al., 1983). The tendency however for the breakthrough curve for the continuum model to be shifted toward slightly larger times relative to the breakthrough curve for the discrete system is observed consistently in all trials.

Our evaluation shows that the shift is caused because the discrete system is slightly non-ergodic as far as mass transport is concerned. Because the sub-domain contains 1344 fracture intersections, we suspect that the non-ergodicity does not occur as a consequence of low fracture densities. However preferential pathways may be developed as a consequence of clustering of the fractures.

The mean and standard deviation on the seepage velocities for a single particle are usually very different than the mean and standard deviation of the swarm of particles. Thus the interchangeability of time and space averages required by the ergodic hypothesis may not always be possible. What apparently is happening is that individual particles moving across the system do not sample the broad range of velocities that can exist in vertical fractures. In the continuum model, each of the particles is forced to sample a larger proportion of lower velocities especially when particles move up or down in the system. Thus, individual particles remain in the continuum slightly longer, delaying breakthrough by a short time. As will be evident in the following section, it is possible to change the way in which statistics are collected in the discrete system in order to lessen the shift between the breakthrough curves.

Approach 2 - Individual Particle Statistics

In this second approach, a logmean velocity and a standard deviation is calculated for a single particle moving through the network. To characterize the entire particle swarm, we calculate the mean and standard deviation for each of the statistics collected for a particle. As expected, the logmean velocities ($-v_1$, $-v_2$, $-v_3$) are equal to those ($-v_1$, $-v_2$, $-v_3$) calculated previously for the swarm of particles. However, there is variability in these means reflected in standard deviations that for one example are 0.15, 0.07, and 0.14 in the three main transport directions. As is apparent, there is usually only minor variability in the mean in direction 2, while in directions 1 and 3 this variability is relatively significant.

The mean of the individual standard deviations in velocity calculated on a particle basis is usually smaller than the comparable statistic calculated for the particle swarm. The standard deviations in a typical simulation calculated as the mean of individual particles are 0.33, 0.24, and 0.32 for directions 1, 2, and 3 respectively. Standard deviations determined from the particle swarm are 0.37, 0.25 and 0.35 respectively.

We are able to modify the manner in which velocities are generated in the continuum to account for this non-ergodic behavior. Having obtained $-v_1$, $-v_2$, and $-v_3$ as before with (1), we can use the new informa-

tion on the variability in these means to generate unique means for each of the reference particles. The probability distributions on velocity that are sampled by a particle moving through the continuum are defined by these means and the mean of the standard deviations calculated on a particle by particle basis. It turns out for the cases we have considered so far that there is relatively small variability in the mean of the standard deviations so that it is not necessary to generate a unique value for each particle as we did with the mean. With the exception of these modifications, particles are moved as before through the continuum.

Figure 4 again compares results between equivalent discrete and continuum problems this time for two examples. Clearly, the results obtained using this modified approach to generating velocity distributions are better than before. Now there is no evidence of a consistent difference between the breakthrough curve for the discrete system and the continuum. The success of these preliminary trials provides evidence that the basic approach we have developed will be applicable to modeling more complex systems.

APPLICATIONS OF THE MODELING CONCEPT

The purpose of this brief section is to demonstrate how the modeling approach we have just described can be applied to a large-scale problem. The domain under consideration is 210 m high and 622.5 m long. The top and bottom of the domain are assumed to be no-flow boundaries, while constant heads are maintained along the two sides to create a mean hydraulic gradient of 0.059. The effective hydraulic conductivity and porosity for the domain are $10^{-7.65}$ m/d and $10^{-4.27}$ m/d respectively. These kind of effective parameters are representative of a fracture network with a geometry similar to that depicted in Figure 2. Thus within the continuum there would be two fracture sets and a total of approximately 5×10^5 fractures and 1.5×10^5 intersections. The two fracture sets are assumed to be oriented parallel and perpendicular to the mean hydraulic gradient. Individual fractures have a logmean aperture of -4.5 m and a standard deviation in aperture of 0.1.

The sub-domain used to collect the necessary statistics on particle motion is exactly 1/100 the area of the continuum. It is also the same as the cases considered earlier in terms of its size, boundary conditions, and fracture geometries. In working with the sub-domain, the distributions on velocities were prepared using the first of the two approaches considered previously. Although using these distributions results in a slight overestimation of breakthrough times for small travel distances, they are probably more appropriate in the much larger continuum. It is highly unlikely that a particle would move over very large distances in a large domain with the characteristics we described in approach 2.

Depicted in Figure 5 are the six distributions that describe particle motion in the sub-domain. Looking at the normalized velocity distributions note first how much more variable the distributions are in directions 1 and 3 as compared to direction 2, and second the tendency for all three distributions to be skewed in the direction of the smaller velocities (normalized values greater than 1.0). The two distributions describing fracture lengths are distinguished by the abundance of fractures less than 1.0 metre and the absence of relatively long fractures. The single distribution describing the frequency of a particle choosing a given transport direction at a decision point is interesting because of the bias that particles have toward moving in direction 2. This bias reflects the fact that direction 2 parallels the orientation of the mean hydraulic gradient and that local gradients for flow in directions 1 and 3 are relatively small.

Using these distributions and assuming a point-source at the mid-point along the upstream boundary, it is possible to simulate transport within this large-scale system. Figure 6 shows the breakthrough curves obtained for the discrete sub-model and the continuum. A comparison of the shape of the two curves suggests that the strong 'tailing' that is apparent in the breakthrough curve for the sub-domain is less marked in the continuum. Initial breakthrough in the continuum occurs at approximately 250 days

with 50% breakthrough at approximately 305 days (Figure 6).

CONCLUSIONS

A new continuum approach has been developed for modeling contaminant transport in large-scale flow systems in fractured rocks. The method is based generally on a moving particle technique where features of particle motion are determined from discrete-fracture simulations on a sub-domain of the system of interest. Because the particle motion is related to the fracture network, the model accounts in a very realistic way for the influence of the fractures.

The ability of the continuum approach to replicate the breakthrough curve for a sub-domain of the same size verifies the basic modeling concept. A few issues in the methodology, related to arguments of ergodicity and the minimum size of the sub-domain, and the nature of boundary conditions for the sub-domain, remain unresolved at present.

The application of the technique to the simulation of a simple, large-scale problem illustrates how the method could be applied to practical problems. The directed motion of reference particles over the large-scale system successfully preserves the unique patterns of mass transport imparted by the fracture geometry. Work is proceeding in this research to extend the approach to systems that are fully two and three-dimensional.

ACKNOWLEDGEMENTS

This research is supported by funds provided by Atomic Energy of Canada Limited as part of the Canadian Nuclear Fuel Waste Management Program.

REFERENCES

Ahlstrom, S.W., H.P. Coote, R.C. Arnett, C.R. Cole, and S.J. Sern, 1977, Multicomponent mass transport model: Theory and numerical implementation (discrete-parcel-random-walk version), Rep. BNWL-2127, Battelle Pac. Northwest Lab., Richland, Wash.

Schwartz, F.W., 1977, Macroscopic dispersion in porous media: The controlling factors, Water Resour. Res., 13(2), 743-752.

Schwartz, F.W., and F.A. Donath, 1980, Scenario development and evaluation related to the risk assessment of high level radioactive waste repositories, U.S. Nuclear Regulatory Comm., NUREG/CR-1609, 158.

Schwartz, F.W., L. Smith, and A.S. Crowe, 1984, Stochastic analysis of macroscopic dispersion in fractured media, Water Resour. Res., 19(5), 1253-1265.

Smith, L., C.W. Mase, D. Chorley, and F.W. Schwartz, 1984, A numerical model for transport in networks of planar fractures, this volume.

Smith, L., and F.W. Schwartz, 1984, An analysis of the influence of fracture geometry on mass transport in fractured media, (in press) Water Resour. Res.

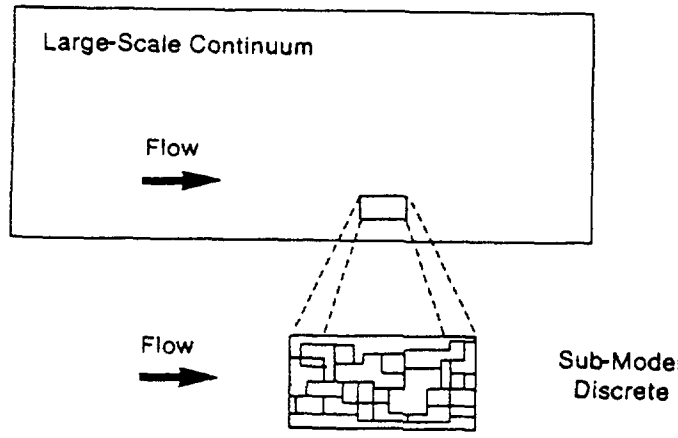

Figure 1. A large-scale continuum with a discrete sub-domain.

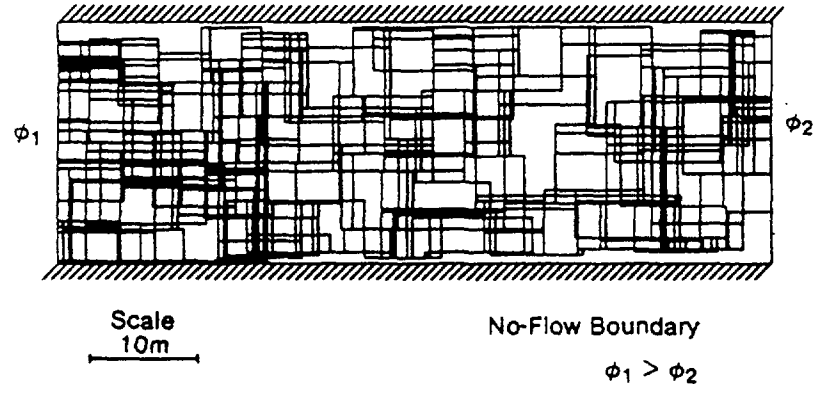

Figure 2. Example of a discrete fracture network generated with two orthogonal fracture sets.

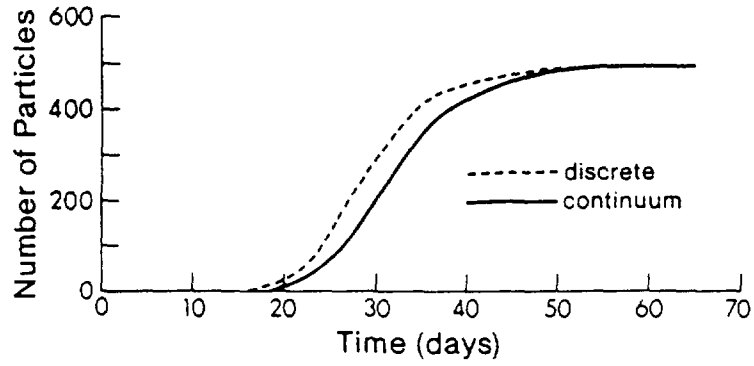

Figure 3. Comparison of breakthrough curves obtained using discrete and continuum (type 1) approaches.

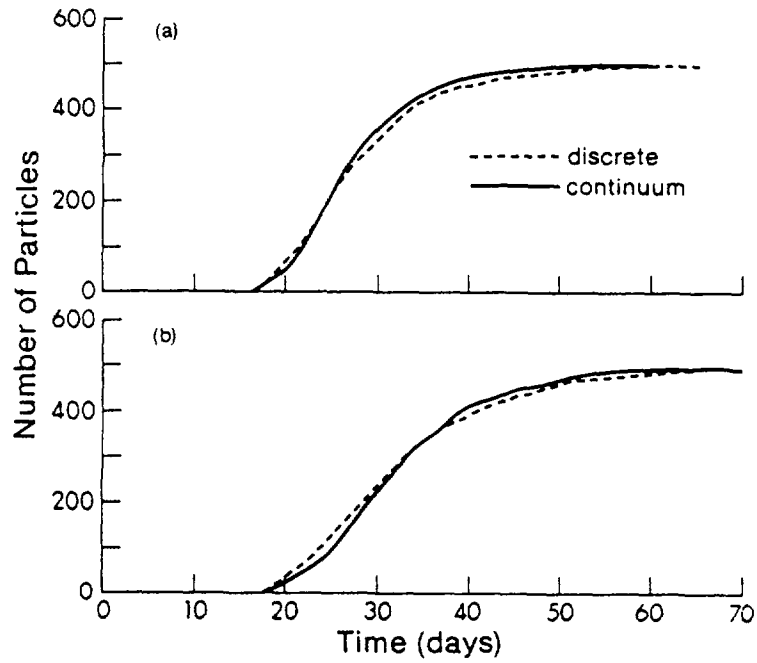

Figure 4. Comparison of breakthrough curves obtained using discrete and continuum (type 2) approaches.

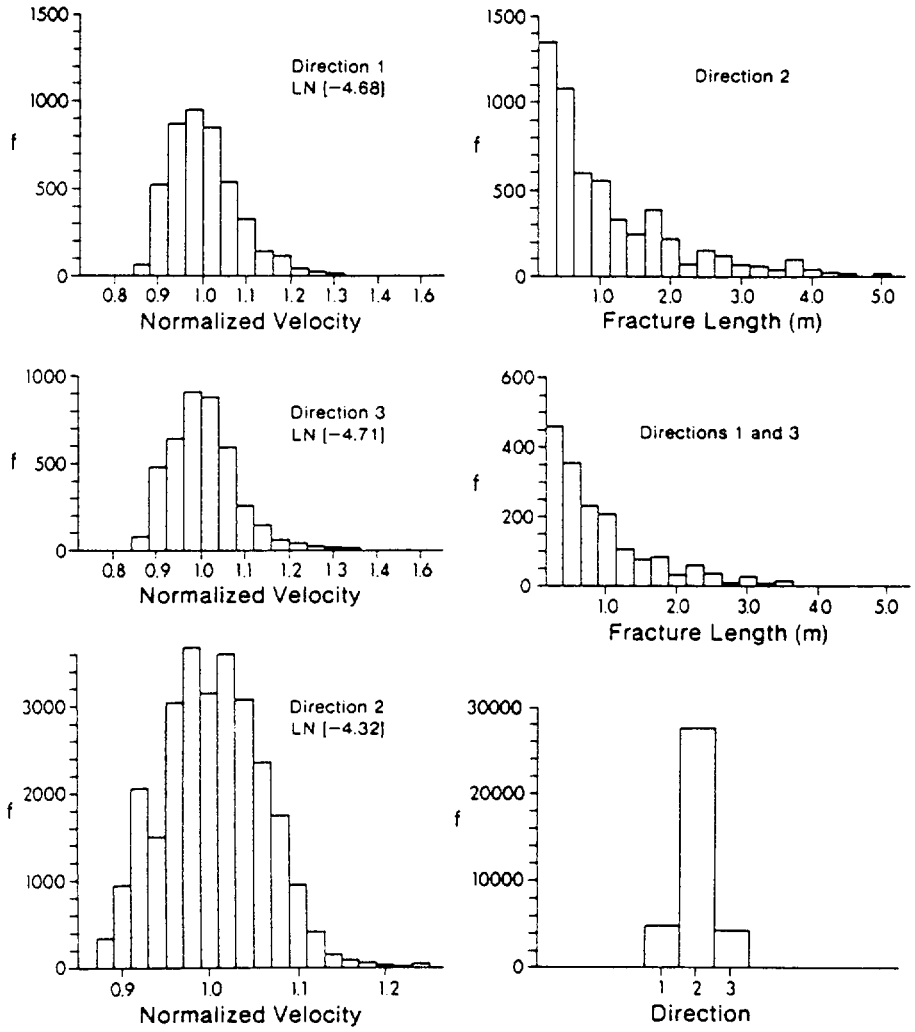

Figure 5. Six distributions defining the essential features of particle motion in a discrete network.

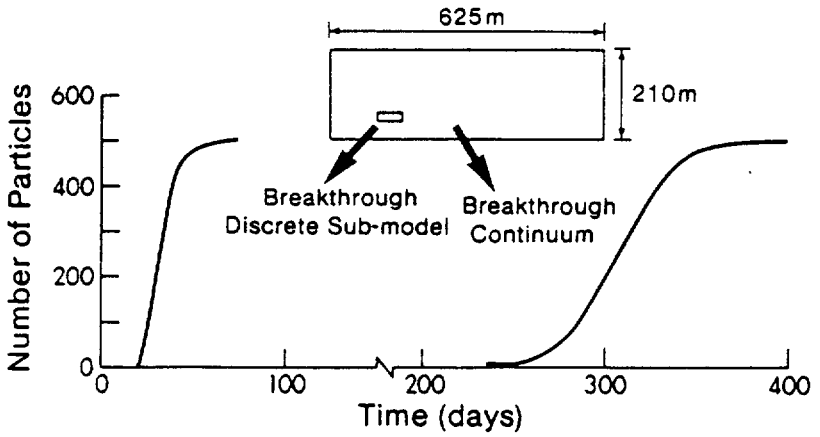

Figure 6. Breakthrough curves obtained for the discrete sub-model and the large-scale continuum.

1775

Schweig, 1986

characteristics whereas the Huato, Sorata, Huayna Potosi, Unduavi and Taquesi batholiths have I-(igneous) type characteristics but with crustal overprints.

The S-type plutons are characterized by their altered appearance, their biotite-muscovite granite composition, their abundance of muscovite over biotite, ubiquitous apatite crystals, and their tourmaline and ilmenite contents. The rocks have high peraluminous indices that range from 1.2 to 1.7. Whole-rock oxygen isotope compositions range from 11.6 to 13.4 o/oo. Quartz and biotite $\delta^{18}O$ analyses are consistent with whole rock determinations.

I-type plutons typically have a fresh appearance, are generally composed of +/-hornblende-biotite granodiorites and high plagioclase biotite granites, lack primary muscovite, and have hornblende and magnetite. Peraluminous indices range from 1.0 to 1.3. Evidence for crustal contamination is contained in their whole-rock oxygen isotope compositions which range from 8.9 to 9.3 o/oo. For an uncontaminated I-type granite, the $\delta^{18}O$ values typically range from 5 to 6 o/oo.

The lack of associated volcanics suggests that the I-type granitoids were emplaced at depths greater than 5 km. But the presence of sedimentary roof pendants and the intimate association of mineralized quartz veins and pegmatites, suggest that erosion has reached just the top of the I-type plutons. Thus the high peraluminous indices may be due to intereactions of the cooling carapace with the overlying sedimentary rocks.

MIOCENE AGE FOR THE ANDESITE AT REEDS CREEK, SACRAMENTO VALLEY, CALIFORNIA | Nº 101924

SAUCEDO, George J., and WAGNER, David L., California Dept. of Conservation, Division of Mines and Geology, 380 Civic Dr., Suite 100, Pleasant Hill, California 94523.

The Reeds Creek Andesite of Clark and Anderson (1938) is exposed along Reeds Creek at the southeastern margin of the Sacramento Valley. They proposed that the andesite pebbles in the Upper Eocene marine Wheatland Formation were derived from the same volcanic source as the andesitic rocks exposed along Reeds Creek, indicating that the andesite at Reeds Creek is older than the voluminous Mio-Pliocene andesites of the western Sierra Nevada. The andesite at Reeds Creek lies stratigraphically above the Eocene Ione Formation and below a rhyolite tuff which Clark and Anderson thought represented typical Sierran rhyolite of Eocene?-Oligo-Miocene age. Along Dry Creek, Wheatland Formation conglomerate contains andesite pebbles and Upper Eocene to Lower Oligocene marine fossils. Dalrymple (1964) reported a "composite age" of 53.5 m.y. from a number of andesite pebbles taken from this conglomerate.

Two new K-Ar ages were determined from samples of the andesite at Reeds Creek. Hornblende from an andesitic block at the top of the exposed section yielded an age of 8.2±0.9 m.y. Plagioclase from an andesite clast in a mudflow breccia near the base of the unit yielded an age of 18±0.5 m.y.

In light of the new K-Ar data and recent correlation of the overlying rhyolite tuff with the Pliocene Nomlaki Tuff, the andesite at Reeds Creek can be considered Miocene in age and probably correlative with the Mehrten Formation. Also, it is unlikely that the andesitic pebbles in the Wheatland Formation are related to the andesite at Reeds Creek.

GEOLOGY OF THE CHICO 1° X 2° QUADRANGLE, CALIFORNIA | Nº 101926

SAUCEDO, George J., and WAGNER, David L., California Dept. of Conservation, Division of Mines and Geology, 380 Civic Dr., Suite 100, Pleasant Hill, California, 94523.

The Chico 1° X 2° quadrangle is the seventh map in the new Regional *Geologic Map Series being prepared by the Division of Mines and* Geology. The quadrangle covers an area of approximately 7,600 square miles in northeastern California and includes parts of the Great Valley and Sierra Nevada geomorphic provinces.

Geologic mapping has progressed rapidly over the past several years in an effort to interpret the complex record of Paleozoic and Mesozoic tectonics preserved within the area. About 75% of this new compilation reflects mapping completed since publication of the 1962 *Olaf P. Jenkins edition of the Chico sheet.*

The Sierra Nevada province occupies roughly 75% of the map. Pre-batholithic rocks in this area can be separated into four northwest-trending belts. (1) A western belt of Jurassic rocks *primarily arc-derived volcaniclastic deposits and ophiolitic rocks of* the Smartville complex. (2) A central belt containing a complex assemblage of disrupted Paleozoic and Mesozoic rocks. (3) The Feather River peridotite belt - a mid to late Paleozoic ultramafic body. (4) *An eastern belt containing several Paleozoic and Mesozoic volcanic arc* complexes and the Lower Paleozoic Shoo Fly Complex. Granitic rocks of the Sierra Nevada batholith make up the balance of the province to the east while to the west it is unconformably overlain by the Cenozoic and Mesozoic deposits of the Great Valley province. Salient geologic features of the northeastern Sacramento Valley include the intensely faulted Chico monocline and the Plio-Pleistocene volcanoes of Sutter Buttes.

Accompanying the geologic map will be a regional cross-section and maps showing: (1) the sources of data used in the compilation and (2) locations and ages of rock samples dated by radiometric methods.

EARLY CRETACEOUS SEDIMENTARY EVOLUTION OF THE SEVIER FORELAND BASIN, MUDDY AND NORTH MUDDY MOUNTAINS, NEVADA | Nº 100954

SCHMITT, James G., Dept. of Earth Sciences, Montana State University, Bozeman, MT 59717 and KOHOUT, Julie B., Dept. of Geoscience, University of Nevada, Las Vegas, NV 89154

Terrigeneous clastic sediments of the Early Cretaceous Willow Tank Formation in southern Nevada record initial development of the Sevier fold-thrust belt and associated foreland basin. The Willow Tank contains a basal conglomerate (5-35m) comprised of massive to crudely horizontally bedded pebble to cobble gravel (Gm) and trough cross-stratified gravel (Gt) with lesser amounts of trough cross-stratified and horizontally stratified sand (St and Sh) lithofacies. Deposition occurred in a Scott-type braided stream complex characterized by development of longitudinal bars and channel lags (Gm), sinuous-crested transverse bars and dunes (Gt and St), and both upper and lower flow regime plane beds (Sh).

The upper portion of the Willow Tank (150m) consists of lenticular sandstone bodies within a mudrock-dominated sequence. Sandstone lenses fine upward, possess basal intraformational lag gravels, and are dominated by medium-scale trough crossbedded sand with ripple cross-laminated sand at their tops. Mudrocks are comprised of interbedded claystone, sandy mudstone, carbonaceous mudshale, and siltstone with interstratified tuffaceous layers. Sandstone units are interpreted to represent meandering stream point bar sequences. Mudrocks were deposited by vertical accretion and ash-fall processes on the adjacent flood plain.

Paleocurrent data from both the basal conglomerate and overlying sandstone lenses indicate a general west-to-east paleoflow direction. Clast-types present include limestone, chert, sandstone, and quartzite derived from erosion of Precambrian-Mesozoic strata. In particular, presence of Precambrian quartzite clasts requires erosion of the distant Wheeler Pass/Gass Peak thrust plate. Such a scenario is supported by the distal fluvial nature of the Willow Tank, suggesting that Early Cretaceous thrusting involved primarily the more distant westerly thrusts.

MESOZOIC THRUST BELT ALONG THE EASTERN EDGE OF YOSEMITE NATIONAL PARK (YNP), CALIFORNIA | Nº 99909

SCHWEICKERT, R. A. AND LAHREN, M. M., Dept. Geol. Sci., University of Nevada--Reno, Reno, NV 89557

New lithologic, stratigraphic, and structural data along with existing mapping suggests that sparsely fossiliferous rocks in a 40 km belt from Molybdenite Creek to Mono Pass consist of the Ord.-Dev. Palmetto Fm, Perm. Diablo Fm, Lower Tr. Candelaria Fm, Lower Jr. Dunlap Fm, and the Golconda allochthon, all overlain by a thick Tr-Jr arc volcanic sequence. Pre-Cenozoic structure is dominated by NW-trending, moderately to steeply dipping, thrust faults that generally parallel bedding and duplicate section. Thrusts commonly are occupied by deformed dacitic to andesitic sills. Most thrusts imbricate the Palmetto-Diablo-Candelaria section, but some interleave Dunlap-equivalent rocks (e.g. Dana seq.) with other units. Structurally lowest rocks occur in the area north of Mono Lake and appear to be part of the Golconda allochthon. Structurally highest rocks at the western edge of the belt are paragneiss, schist, marble, and amphibolite possibly derived from the Tr-Jr volcanic section, and quartzite, orthogneiss, and ultramafic rocks of unknown origin. Transport direction for the thrusts, uncertain in detail, probably was easterly. Some thrusts (e.g. Lundy Canyon thrust) are cut by 200 m.y. plutons, others are related to regionally developed Nevadan(?) cleavage, and others (e.g. Gaylor Peak thrust) involve Dunlap-equivalent rocks that may be as young as Cretaceous (Kistler and Swanson, 1981). These thrusts near the eastern edge of YNP probably are a continuation of the Luning-Pamlico thrust belt (oldow, 1983), dextrally offset about 110 km on EW faults (Stewart, 1985). This Mesozoic backarc thrust belt, when traced westward to the arc, turns southward, parallels the arc axis, and cuts across the Golconda thrust and into the underlying Roberts Mts. allochthon. The southern extent of the thrust belt is not known, but repetition of section in the Ritter and Goddard areas (Tobisch et al., 1985) may indicate the thrust belt extends into those areas.

1775

THE INCEPTION OF BASIN AND RANGE TECTONICS IN THE REGION BETWEEN DEATH VALLEY AND THE SIERRA NEVADA, CALIFORNIA | Nº 102889

SCHWEIG, Eugene S., III, Tennessee Earthquake Information Center, Memphis State Univ., Memphis, TN 38152

In the area of the southwestern Great Basin from the Panamint Range to Owens Valley, the inception of Basin and Range tectonic activity generally proceeded from east to west and then spread north and south. The evidences for this conclusion include volcanic activity, initiation of normal faulting, and sediment type and provenance.

In the Panamint Range, uplift, normal faulting, and silicic plutonism began at least 13 Ma. Sediments were shed as far westward as the present-day Argus and Saline Ranges.

Between 7 and 8 Ma volcanism began on the Darwin Plateau at the northeastern edge of the Argus Range, with extensive basalt flows on a relatively flat surface. Volcanism spread westward reaching the southern Inyo Mountains about 6 Ma. By this time eastward tilting of the Argus Range had progressed to the point that debris flow deposits derived from the Panamint Range ceased and locally derived sediments were being deposited. Demonstrable normal faulting began on the Darwin Plateau by about 6 Ma. Between 5 and 6 Ma a volcanic field stretched from the northern Panamint Range to the southern Inyo Mountains. By 4 Ma

volcanism had been reduced to a few scattered localities in this field. At the western edge of the field volcanic activity spread north to the Saline Range and south to the Coso Range.

By 3.0 to 3.5 Ma break-up of the area into its present geography was essentially complete.

STABILIZATION OF FRIENDLY VALLEY LANDSLIDES, CANYON COUNTRY, LOS ANGELES COUNTY, CALIFORNIA, A CASE STUDY. № 99932

SCULLIN, Michael, SIMON, David, Robert Stone & Associates, Inc., 15414 Cabrito Road, Unit A, Van Nuys, CA 91406-1439

Numerous landslides have been identified in the Friendly Valley area of Newhall, California. Some of these slides are located in a burgeoning population center and increase tne high-geologic-risk of urban development.

The case study investigation involved approximately 30± acres of landsliding. A maximum of three distinct slide planes were identified varying in thickness of 20± feet to 90± feet. Slope stability analysis for the entire mass indicates a factor of safety below the minimum standard 1.5.

Stabilization of the slide masses will require extensive buttressing along the toe of the slide, a shear key buttress above the Sierra Highway that crosses the slide and possibly additional shear key buttressing in an area where the County proposes the Golden Valley Parkway that may cross the upper portion of the slide. The upper 20± feet of inplace slide mass will be recompacted to minimize infiltration. Extensive subdrainage and surface drainage control will be necessary as an added safety measure.

MICROTERRANES WITHIN THE CEDROS COMPLEX, CEDROS ISLAND, CENTRAL BAJA CALIFORNIA № 90532

SEDLOCK, Richard L., Dept. of Geology, Stanford Univ., Stanford, CA 94305

Disrupted metamorphic rocks of the Cedros Complex on Cedros Island are assigned to several terranes characterized by different metamorphic histories and protlith assemblages. Contacts among individual terranes, as well as between the Cedros Complex and other Mesozoic units on Cedros, are well-exposed faults marked by serpentinite.

Terrane 1 consists of completely recrystallized, regionally metamorphosed metavolcanic and metasedimentary rocks that exhibit jadeitic cpx, sodic amphibole, and lawsonite. These blueschist facies rocks probably were subducted to depths of at least 20 km prior to accretion to (underplating of?) an ancient subduction complex.

Terrane 2 consists primarily of quartz-rich turbidites that contain abundant lawsonite and rarer incipient jadeite while retaining original clastic textures. This terrane probably represents trench deposits subducted to moderate depths (10-20 km) prior to accretion.

Terrane 3 consists mainly of volcanic rocks interbedded with red chert and fine-grained terrigenous rocks. Microprobe analysis of cpx from the volcanic rocks indicates alkaline affinities.

Finally, rare eclogite and coarse-grained schist and gneiss (blueschist facies) present in eroded pods along part of the fault boundary of Terrane 1 are products of high-pressure, moderate-temperature metamorphism and may be tectonic blocks exhumed from depth within a major fault zone.

Differences in inferred P-T trajectories for the above terranes suggest substantial (vertical) displacements on the major faults that bound them. The timing of motions on these faults has not yet been determined, however.

STRUCTURAL DEVELOPMENT AT THE NORTHERN MARGIN OF THE DOONERAK DUPLEX, BROOKS RANGE, ALASKA № 101236

SEIDENSTICKER, C.M., Dept. of Geology and Geophysics, Rice University, Box 1892, Houston, TX 77251

In the vicinity of Mt. Doonerak in the central Brooks Range, the Blarney Creek Thrust (BCT) separates a package of lower Paleozoic rocks which lie to the south (below the thrust) from a package of upper Paleozoic rocks which lie to the north (above the thrust). The BCT was formed initially within the Mississippian Kayak Shale as a basal décollement surface above which upper Paleozoic rocks were imbricated during an early stage of Brookian contraction. During continued progressive deformation, deeper thrust faults involving lower Paleozoic rocks ramped up into the Kayak Shale and merged with the pre-existing BCT to form a duplex structure; the BCT then became the roof thrust during duplex development. Emplacement of lower Paleozoic horses into the duplex resulted in folding of the imbricated upper Paleozoic section into an antiform. This model accounts for the observed distribution of bedding and cleavage, which dip north above the BCT but which dip south below the BCT; it also explains the juxtaposition of younger over older rocks at the thrust fault.

The Mississippian Kekiktuk Conglomerate, a thin competent unit lying conformably below the Mississippian Kayak Shale and unconformably above the lower Paleozoic rocks, was sometimes caught up in early imbricate stacking of the upper Paleozoic section, but more often it remained behind with the lower Paleozoic rocks during this stage of structural development because detachment was apparently more easily accommodated just above in the Kayak Shale. During later duplex development, the Kekiktuk locally became interleaved with thin slices of lower Paleozoic rock in the BCT zone.

A MODEL FOR THE STRUCTURAL EVOLUTION OF THE CENTRAL DEATH VALLEY BASIN FROM COCORP SEISMIC DATA № 97590

SERPA, Laura, Earth Sciences, Univ. of New Orleans, NO, LA 70148
DE VOOGD, Beatrice, Cornell, Ithaca, NY 14853, WRIGHT, Lauren, Penn. State, University Park, PA 16802, and TROXEL, Bennie, UC Davis, Davis, CA 95616.

COCORP deep seismic reflection profiles in the vicinity of Death Valley, California, provide information on the block faulting associated with the active subsidence of the central Death Valley basin. Both the surface and seismic data indicate two distinct levels of faulting. Shallow faults (less than 4 km deep) appear to terminate near the top of the crystalline basement and, thus, are interpreted to be the result of the collapse of the layered rocks above the tilting crystalline fault blocks. Other faults can be traced in the seismic data to depths of 10 to 15 km and these appear to bound large crystalline fault blocks. Thus these deep faults are related to the regional extension of Death Valley.

The combined surface and seismic data indicate the zones of deep faults trend in 4 directions near the southern end of the basin. The predominantly normal faults trend N-S or NE-SW and the predominantly strike-slip faults trend NW-SE or E-W. Faults with all of the above orientations have been active during time of the subsidence of the central Death Valley basin (the last 6 m.y.). A reconstruction of the movement of upper crustal blocks bounded by these faults indicates the basin subsidence to be the result of the simultaneous rotation of north-trending fault blocks about a subhorizontal axis (i.e. the N-S normal faults and E-W strike-slip faults) and horizontal translation of the Panamint block relative to the Black Mountain block (the NW-SE strike-slip faults and the NE-SW normal faults). At the base (15 km) of the upper crustal fault blocks there is a subhorizontal zone of detachment which appears to continue from the northern Mojave desert, across Death Valley, to the Nopah Range. In the Mojave desert and east of the Nopah Range, this detachment appears to dip down to the Moho.

DISTRIBUTION AND SLOW CALCIFICATION IN *ALVEOLINELLA QUOYI*: IMPLICATIONS FOR FUSULINID PALEOBIOLOGY № 87701

SEVERIN, Kenneth P., and LIPPS, Jere H., Department of Geology, University of California, Davis, CA 95616

Growth rates and habitat distribution of the living large fusiform foraminifera, *Alveolinella quoyi*, may serve as a model to understand the paleobiology and test accumulation rates of extinct alveolinids and fusulinids. To date only Recent large discoidal foraminifera have provided a basis for inference, although they may differ in habitat and calcification rates.

In *A. quoyi*, calcification procedes much slower than in the discoidal forms. Although this species harbors algal endosymbionts, calcification is affected by light to only a minor degree. An herbicide, which completely inhibits calcification in other symbiont bearing organisms, depresses but does not stop calcification. Thus, calcification in *A. quoyi* is less affected by the presence of symbionts than it is in other symbiont-bearing tropical foraminifera.

Calcification rates of typical specimens indicate that a 3mg adult is three to five years old, older than estimated ages for most discoidal forms. At Papua New Guinea, individuals live only in very certain areas on algal-covered substrates, usually coral rubble. Despite the restricted distribution of living individuals, dead tests are common in the unconsolidated sediments throughout the lagoon.

The combination of slow calcification and restricted life habitat imply that *A. quoyi* tests are added to the sediment slowly. Because dead tests are common in lagoon sediments, they appear to persist for a long time. The lower density of dead tests compared with the common carbonate sedimentary particles may help tests survive destruction and desperse them widely.

Large accumulations of *A. quoyi* tests may be quite old and do not indicate life assemblages or habitats. Similarly, large fusulinid deposits may have been formed by long-term accumulation of slow-growing tests which were relatively resistant to destruction and which lived elsewhere.

THE SADDLE ISLAND DETACHMENT FAULT, LAKE MEAD, NEVADA: UPPER PLATE GEOLOGY AND REGIONAL SIGNIFICANCE № 96064

SEWALL, Angela and SMITH, E.I., Department of Geoscience, University of Nevada, Las Vegas, NV 89154

On Saddle Island a mid-Tertiary detachment fault separates two lithologically and structurally different terranes. In the upper plate, flows of mid-Tertiary dacite are separated from the Precambrian basement by a conglomerate of Tertiary age containing clasts of Paleozoic carbonate and quartzite, and Precambrian basement. The Precambrian basement consists of amphibolite and schist intruded by basalt and dacite of Tertiary age and diorite (age unknown). Foliation in upper plate amphibolite and schist trends to the north, dips steeply and appears to be unfolded. In contrast, in the lower